Table 2 Statistically derived variations

Range of values ($W_{nominal} = 1$)	Probability that actual weight is included in range (%)
0.83–1.21	50
0.75–1.33	68.3
0.58–1.74	95

for conventional materials. Thus, a general expression for parachute weight may be stated as

$$W_{chute} \approx k_1 N P_s l_s + k_2 P_c D_0^2 \quad (1)$$

Canopy strength will be compatible with total line strength for a well-designed chute. Thus, P_c may be taken as approximately proportional to NP_s. In addition, l_s is directly proportional to D_0 for conventionally configured parachutes. With these considerations, Eq. (1) may be restated in the form

$$W_{chute} \approx k_3 N P_s D_0 (1 + k_4 D_0) \quad (2)$$

Thus, $W_{chute} \propto NP_sD_0$ if $k_4 D_0 \ll 1$.

Correlation of Data

Table 1 lists weight and configuration data obtained from various sources[1–3] for 59 parachutes. Most of these chutes are of relatively conventional construction with $l_s/D_0 \approx 1$ and $N \approx D_0$ expressed in feet (at least for $D_0 > 10$ ft). Figure 1 shows weight vs NP_sD_0 on log-log scales for the parachutes of Table 1. The straight line shown in Fig. 1 is

$$W(\text{lbm}) = 0.57 \times 10^{-4} [NP_sD_0(\text{lbf-ft})]^{0.96} \quad (3a)$$

or

$$W(\text{kg}) = 1.9 \times 10^{-5} [NP_sD_0(\text{N} - \text{m})]^{0.96} \quad (3b)$$

The data scatter in Fig. 1 appears due as much to variations within each specific type of chute as to type-to-type variations. Thus, the incorporation of all types of chute in one graph appears valid.

Statistical methods[4] applied to the data of Table 1 permit calculation of the variations and associated probabilities indicated in Table 2.

The spread associated with the calculated nominal value for chute weight tends to be large, but some of the spread is attributable to the inclusion of unconventional chute configurations in the data. Since 50% of the data are within +21%, −17% of the nominal, the nominal weight value of Eqs. (3) multiplied by 1.21 should provide a fairly conservative maximum weight for estimating purposes. Note, however, that the weights of Table 1, Fig. 1, and Eqs. (3) are for the parachute only; that is, riser, deployment bag, and special attachment link weights are excluded. Riser weight may be estimated as indicated in a previous work.[5]

Differentiation of the logarithm of Eqs. (3) gives the variation in W for small variations in N, P_s, and D_0. For most chute applications, $F_0 \propto qS_0$ for small changes in deployment conditions and $NP_s \propto F_0$. Thus, $NP_s \propto qD_0^2$. Use of this relationship in Eqs. (3) and differentiation of the logarithm of the result can be used to obtain the variation in W for small variations in q and D_0.

References

[1] Pepper, W. B., Jr., "Parachute Design and Performance for Supersonic Deployment and for the Recovery of Heavy Loads," DGLR-DFVLR-AGARD Symposium, Sept. 15–19, 1969, Technical University of Braunschweig, Braunschweig, West Germany.

[2] "X-7A Supersonic Ramjet Test Vehicle Parachute Recovery System," TR 55-162, June 1955, Wright Air Development Center, Wright-Patterson Air Force Base, Ohio.

[3] Lindgren, M. J., private communication, May 1970.

[4] Arkin, H. and Colton, R. R., *Statistical Methods*, 4th ed. revised, Barnes & Noble, New York, 1956, Chaps. IX and X.

[5] French, K. E., "Drogue Parachute Weight," *Astronautics and Aerospace Engineering*, Vol. 1, No. 5, June 1963, pp. 94–95.

Equilibrium Vortex Positions

DONALD D. SEATH*
The University of Texas at Arlington, Arlington, Texas

VORTICES on the lee side of inclined cylindrical and conical bodies can cause significant departures of experimental data from inviscid slender-body theory. These vortices appear symmetrically in pairs, starting near the nose and growing in size and distance from the body as they trail downstream. Tinling and Allen[1] found one pair of counter-rotating vortices behind an ogive-cylinder body at subsonic speeds. Rainbird et al.[2] found up to three pairs of vortices behind an inclined circular cone in a water tunnel.

An examination of these body vortex flowfields in a plane perpendicular to the body axis (the crossflow plane) reveals a circular body with one, two, or three pairs of vortices on the lee side, and a crossflow velocity $U = V\sin\alpha$, where V is flight velocity and α is angle of attack. An idealized potential flow equation can be written for this flowfield, and, for the case of only one pair of vortices in the wake, an analytical solution has been obtained by Föppl[3] for the equilibrium positions of these wake vortices. Details of this solution are given by Milne-Thomson.[4]

This Note presents equations and solutions for the equilibrium positions of multiple pairs of vortices in the wakes of circular and elliptic bodies.

Analysis

The complex potential for N pairs of vortices (and their images) of strength Γ_j, a doublet to represent a circular body of radius a, and a uniform stream of velocity U is (see Fig. 1)

$$w(z) = U\left(z + \frac{a^2}{z}\right) + \sum_{j=1}^{N} \left(\frac{i\Gamma_j}{2\pi}\right)\left[\ln(z - z_j) - \ln\left(z - \frac{a^2}{z_j^*}\right) - \ln(z - z_j^*) + \ln\left(z - \frac{a^2}{z_j}\right)\right] \quad (1)$$

where z^* is the complex conjugate of z. At an arbitrary point z_k, coinciding with one of the N vortices in the first quadrant,

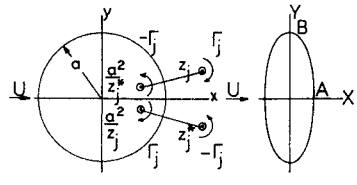

Fig. 1 Circle plane and ellipse plane.

Received August 17, 1970; revision received October 13, 1970. This work was supported in part by the National Science Foundation under Grant GK-940.

* Associate Professor of Aerospace Engineering. Associate Member AIAA.

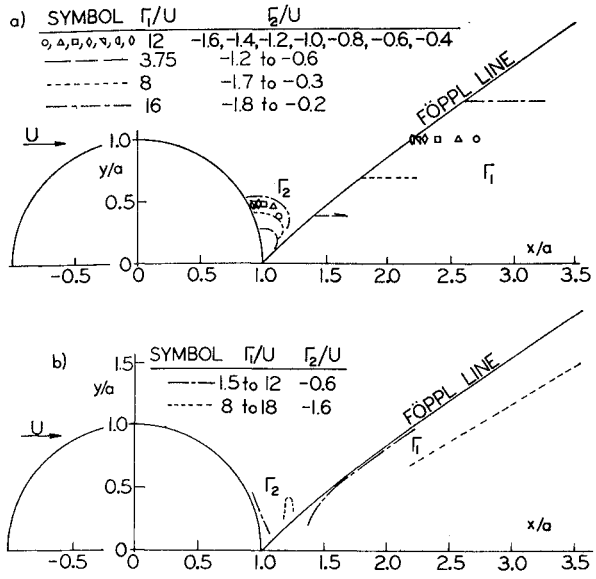

Fig. 2 Equilibrium positions for two pairs of vortices behind a circular cylinder.

the induced velocity is

$$Q_k = \left[\frac{dw}{dz} - \left(\frac{i\Gamma_k}{2\pi}\right)(z - z_k)^{-1}\right]_{z=z_k} = \left\{U\left(1 - \frac{a^2}{z^2}\right) + \sum_{j=1}^{N}\left(\frac{i\Gamma_j}{2\pi}\right)\left[(z - z_k)^{-1} - \left(z - \frac{a^2}{z_j^*}\right)^{-1} - (z - z_j^*)^{-1} + \left(z - \frac{a^2}{z_j}\right)^{-1}\right] - \left(\frac{i\Gamma_k}{2\pi}\right)(z - z_k)^{-1}\right\}_{z=z_k} \quad (2)$$

The equilibrium position of a vortex is defined as the position where the induced velocity is zero. Therefore, Eq. (2) is equated to zero and solved for z_k for each of the N vortices present, providing the equilibrium position for each vortex present in the flowfield. The Newton-Raphson iteration technique may be used to solve this set of equations numerically for assumed values of Γ_j/U.[5]

The flowfield in the region exterior to the circle $r = a$ in the z plane may be conformally mapped onto the region exterior to an ellipse in the $Z = X + iY$ plane (see Fig. 1) by the transformation

$$Z = z + (A^2 - B^2)/4z \quad (3)$$

where A and B are the semielliptic axes in the X and Y directions, respectively. Velocities at corresponding points in the two planes are related by the derivative dz/dZ of the transformation in the usual fashion of potential theory, except at the vortex locations where the theoretical method outlined by Lin[6] is used, giving the velocity at Z_k as

$$P_k = [Q_k z' + (i\Gamma_k/4\pi)(z''/z')]_{Z=Z_k} \quad (4)$$

where the primes indicate differentiation with respect to Z.

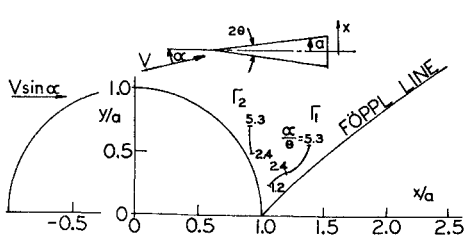

Fig. 3 Vortex positions for a circular cone in water.[2]

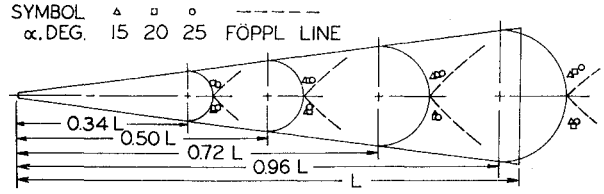

Fig. 4 Vortex positions at four axial stations for an inclined 15° circular cone in a low-speed wind tunnel.[7]

To find the equilibrium vortex positions in the wake of an elliptic cylinder, the following procedure is used: 1) specify A,B,N, and Γ_k/U, for $k = 1,2, \ldots, N$; 2) arbitrarily choose initial values of the vortex positions Z_k in the ellipse plane; 3) calculate the corresponding vortex positions in the circle plane z_k by Eq. (3), velocity at each z_k by Eq. (2) with $a = (A + B)/2$, and induced velocity at each Z_k by Eq. (4); 4) use Newton-Raphson method to obtain corrections, ΔZ_k; and 5) calculate new values of Z_k by adding ΔZ_k's to old values of Z_k. Repeat steps 3–5 until velocities $|P_k| \leq \Delta U$. A value of $\Delta U = 0.00133U$ was used for results presented.

Results

Calculated equilibrium positions for one pair of vortices in the wake of a circular body coincided with the explicit analytical positions found by Föppl.[3] Equilibrium positions for two pairs of vortices of various strengths in the wake of a circular cylinder are presented in Fig. 2. The point symbols in Fig. 2a show equilibrium positions for 7 values of Γ_2/U when $\Gamma_1/U = 12$. The Föppl line is shown for reference purposes. Only half of the plane is shown because the flowfield is symmetrical with respect to the x axis. The curve symbols in Fig. 2a show the results of similar calculations with $\Gamma_1/U = 3.75$, 8, and 16, which illustrate the streamwise movement of the primary vortex equilibrium position when the magnitude of the secondary vortex is increased. Fig. 2b presents the equilibrium vortex positions when Γ_1 is varied while holding Γ_2 constant; the paths of the primary vortex positions in these cases are nearly parallel to the Föppl line. These different vortex paths may furnish a possible explanation for those observed experimentally. For example, the primary vortex behind a circular cone moved away from the cone as α (and Γ) increased (see Fig. 3).[2] At low α's, the locus of primary vortex positions is nearly parallel with the Föppl line. But, as α reaches moderate values, the presence of a secondary (counter-rotating) vortex-pair is observed, and the locus of primary vortex positions changes to a direction nearly parallel to the x axis, similar to the trend in Fig. 2a. At high α's, the direction changes back to one approximately parallel to the Föppl line, similar to Fig. 2b.

Another test[7] showed that the pattern of primary vortex positions varied with axial position along a finite 15° circular cone in a low-speed wind tunnel (see Fig. 4). For the two forward stations examined, the line of vortex positions (as viewed in the crossflow plane) is in a nearly streamwise direction (x direction). Whereas, at the aft station, the line

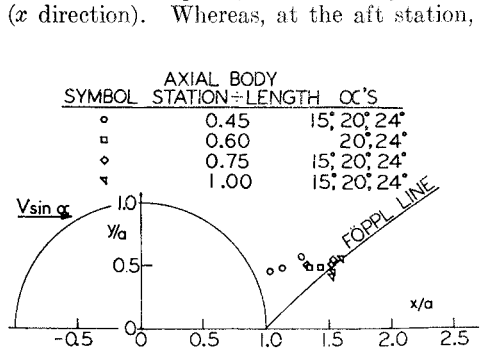

Fig. 5 Vortex positions for an ogive-cylinder in low-speed wind-tunnel test by Tinling and Allen.[7]

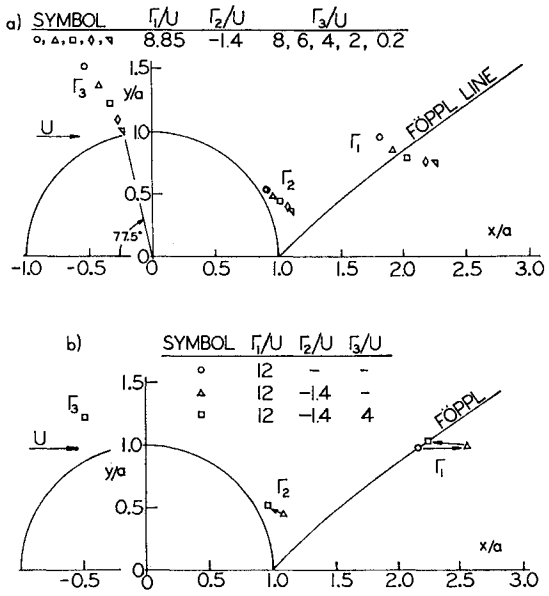

Fig. 6 Equilibrium positions for three pairs of vortices behind a circular cylinder (top), and effects of adding second and third vortex pairs (bottom).

of vortex positions is nearly parallel to the Föppl line. The coarse measurement methods of Ref. 6 did not detect secondary and tertiary vortices in the flow field, the presence of which might explain the primary vortex patterns observed.

Consider, also, the data of Tinling and Allen[1] for an inclined ogive-cylinder model in a low-speed wind-tunnel test, as plotted in Fig. 5 for several axial stations. The locus of vortex positions with increasing α is nearly parallel with the x direction, not the Föppl line. This suggests that the actual

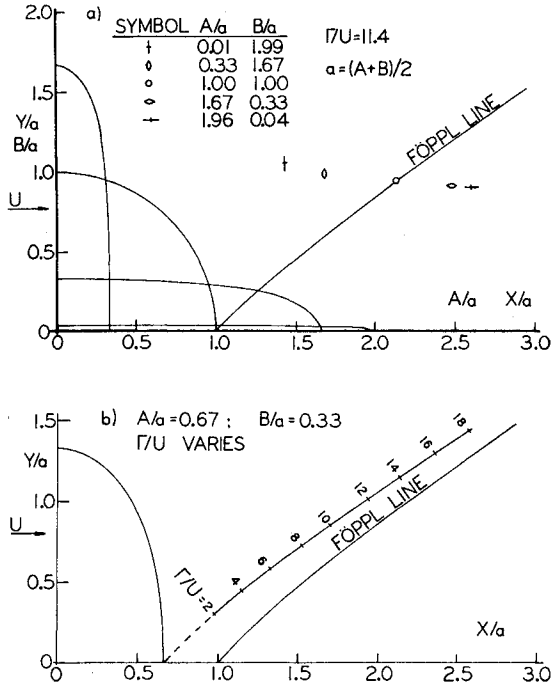

Fig. 7 Equilibrium positions for one pair of vortices behind a series of elliptic cylinders (top), and effect of Γ/U on equilibrium vortex positions behind an elliptic cylinder (bottom).

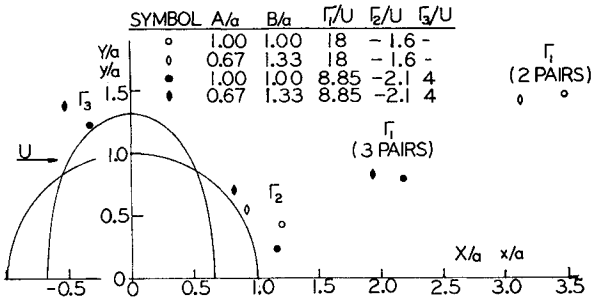

Fig. 8 Comparison of equilibrium positions for two and three pairs of vortices behind circular and elliptic cylinders.

flowfield may not be adequately represented by a potential flow analytical model containing a single pair of vortices in the wake, but rather it may be necessary to include two or more pairs of vortices in the wake (see Fig. 2).

Equilibrium vortex positions were calculated for three pairs of vortices in the wake of a circular cylinder. The strength of each pair was, in turn, varied while the other two pairs were held constant. Figure 6a shows a typical result; as the strength of the tertiary vortex decreased, its equilibrium position moved toward the circular cylinder in a nearly radial direction. The extrapolation of this line intersects the circle 77.5° from the upstream stagnation point. Other calculations[5] show that this angular intercept decreases when the magnitude of the secondary vortex is decreased. Schlichting[8] gives a calculated separation position of 81.5° for laminar boundary-layer flow about a circular cylinder. Although the agreement may be fortuitous, the correlation of these two results is deserving of future investigation.

Figure 6b compares the vortex equilibrium positions for one, two, and three pairs of vortices with the same primary and secondary vortex strengths. When the secondary vortex is added, the primary vortex moves (as indicated by the arrow) to the right. When the third vortex is added, the primary and secondary vortices move to the left and slightly upward. The fact that the primary vortex returns to the Föppl line when the third vortex is added occurs only for this combination of vortex strengths.

The equilibrium vortex positions for one pair of vortices behind a series of elliptic cylinders are presented in Fig. 7a. The elliptic cylinder cross section was varied from a vertical (nearly flat) plate to a horizontal (nearly flat) plate. The equilibrium position for the circle is on the Föppl line, and it moves upstream and slightly farther from the X axis when the major axis of the ellipse is transverse to the freestream flow; when the major axis is parallel to the flow, it moves downstream.

As may be shown analytically, the equilibrium vortex position in the presence of a flat plate parallel to the flow is independent of X, and its Y position depends on Γ/U. Figure 7b presents the equilibrium positions for a single pair of vortices of various strengths, behind an elliptic cylinder with relative major semiaxis of 1.33, transverse to the flow, and relative minor semiaxis of 0.67, parallel to the flow. The locus of equilibrium positions forms a line that is similar to the Föppl line. The two lines converge as $\Gamma/U \to \infty$.

Figure 8 shows the effect of changing the body cross section from circular to elliptic on the equilibrium positions for multiple pairs of vortices.

References

[1] Tinling, B. E. and Allen, C. Q., "An Investigation of the Normal-Force and Vortex-Wake Characteristics of an Ogive-Cylinder Body at Subsonic Speeds," TN D-1297, 1962, NASA.

[2] Rainbird, W. J., Crabbe, R. S., and Jurewicz, L. S., "A Water Tunnel Investigation of the Flow Separation about Circu-

lar Cones at Incidence," Rept. LR-385, NCR-7633, 1963, National Research Laboratories, Ottawa, Canada.

[3] Föppl, L., "Wirbelbewegung hinter einem Kreiszylinder," *Sitzungsberichte der Bayerischen Akademie der Wissenschaften zu Munchen*, Munich, Germany, 1913, pp. 1–17.

[4] Milne-Thomson, L. M., *Theoretical Hydrodynamics*, 4th ed., Macmillan Co., New York, 1960, pp. 367–369.

[5] Seath, D. D., "Equilibrium Vortex Positions in the Wake of Circular and Elliptic Bodies," Rept. AE 70-01, 1970, The University of Texas at Arlington Engineering Research, Arlington, Texas.

[6] Lin, C. C., "On the Motion of Vortices in Two Dimensions," Applied Mathematics Series No. 5, 1943, University of Toronto, Toronto, Canada.

[7] Seath, D. D., "Vortex Wake Investigation of An Inclined 15-Degree Circular Cone At Low Speeds," 1969, *The University of Texas at Arlington Engineering Research Report*, Arlington, Texas.

[8] Schlichting, H., *Boundary Layer Theory*, 4th ed., McGraw-Hill, New York, 1960, p. 252.

Estimation of the Maximum Temperature of a Swept Leading Edge for an Equilibrium Glide Entry

Davis H. Crawford*
NASA Langley Research Center, Hampton, Va.

INTEREST in the space shuttle with a large lateral range capability has prompted several designers to propose swept- or delta-winged configurations. A simple relation for estimating the maximum stagnation line temperature on the wing leading edge during an equilibrium glide entry is derived herein. This relation, amenable to hand calculation, is based on a modified form of the Detra, Kemp, and Riddell relationship[1] for the laminar heating (Btu/ft²-sec) to the stagnation point of a sphere of radius R:

$$q_{s,0} = 868(\rho/\rho_0 R)^{1/2}(10^{-8}u^2)^{1.575}\xi \tag{1}$$

where $\xi = [2C_p(T_\infty - T_w) + u^2]/[2C_p(T_\infty - 540) + u^2]$ and where ρ, ρ_0, C_p, and T_∞ are the local density, the sea-level density, the specific heat, and the temperature of the air, and where T_w and u are the vehicle wall temperature and the flight velocity. The atmospheric density variation, $\rho = \rho_k e^{-\beta a}$, is that suggested by Chapman in Ref. 2 where the reference density, $\rho_k = 0.087$ lb/ft³, together with a value of $\beta = 1/23{,}500$ provides satisfactory accuracy in the altitude range a of current interest. The velocity (fps) determined by equating the sum of the aerodynamic lift and centrifugal forces to the weight of the vehicle, is

$$u^2 = [(R_E + a)gB]/[(R_E + a)\rho/2 + B] \tag{2}$$

where R_E is the radius of the earth (20.9×10^6 ft), and $B = W/SC_L$, where W, S, and C_L are the weight, planform area, and lift coefficient of the vehicle.

The stagnation-line heating on a swept cylinder is related to the stagnation-point heating on a sphere by the factor $2^{1/2}$, and the function $\cos^{1.1}\Lambda_e$, Refs. 3–4, where Λ_e, the effective sweep angle, is $\sin^{-1}(\cos\alpha \sin\Lambda)$. Thus, the heat transfer to the swept-wing leading edge appears as follows:

$$q_s = q_{s,0}(\cos^{1.1}\Lambda_e)/2^{1/2} \tag{3}$$

At maximum heating the derivative of q_s with respect to a in Eq. (1) or Eq. (3) vanishes (ρ and u are functions of a, but the temperature variation is trivial). The corresponding values of altitude and velocity are

$$a = -(1/\beta)\ln[(2g/\rho_k u^2)B\eta]\text{ft} \tag{4}$$

where

$$\eta = [\beta(R_E + a) - (3.15 + 2\varphi)]/\{[\beta(R_E + a) - 1](3.15 + 2\varphi)\}$$

$$\varphi = [2C_p(T_w - 540)u^2]/[2C_p(T_\infty - T_w) + u^2][2C_p(T_\infty - 540) + u^2]$$

and

$$u^2 = g\zeta \tag{5}$$

where

$$\zeta = [\beta(R_E + a)^2](2.15 + 2\varphi)/[\beta(R_E + a) - 1](3.15 + 2\varphi)$$

When the maximum convected heat transfer from Eq. (3) is set equal to the radiated heat transfer, the stagnation-line temperature is given by

$$T_w^4 = (868/\sigma)[(2g/\rho_0 u^2)\eta]^{1/2}(10^{-8}u^2)^{1.575}\xi(B/R\epsilon^2)^{1/2} \times (\cos^{1.1}\Lambda_e)/2^{1/2} \tag{6}$$

where σ and ϵ are the Stefan-Boltzmann radiation constant and the emissivity, and the sea-level density is given[5] as $\rho_0 = 0.0765$ lb/ft³.

Iteration is necessary to evaluate u, a, and T_W. The convergence is rapid since the terms which call for iteration have a minor effect, and average values can be used with little error. For instance, the velocity u at which maximum heating occurs varies only in the narrow range from 21,650 fps to 21,680 as W/SC_L is varied from 40 to 320; similarly, a and T_W vary over a narrow span as a function of W/SC_L.

The foregoing discussion suggests the simplification of Eqs. (4–6) by evaluating constant terms, by selecting nominal values of terms which vary slightly, and by dropping negligible terms. With an assumed wall temperature of 3000°R and an assumed stream temperature of 400°R, the following simplified relations for peak heating may be found:

$$u = 21{,}650 \text{ fps} \tag{7}$$

$$a = 233{,}200 - 23{,}500 \ln(10^{-2}B)\text{ft} \tag{8}$$

$$T_w = 3202(10^{-2}B/R\epsilon^2)^{1/8}\cos^{0.275}\Lambda_e{}^\circ\text{R} \tag{9}$$

for a swept-cylinder leading edge, and

$$T_w = 3492(10^{-2}B/R\epsilon^2)^{1/8}{}^\circ\text{R} \tag{10}$$

for a sphere stagnation point. Thus, with $B = 100$ lb/ft², $R = 1$ ft, $\epsilon = 1.0$, and $\Lambda_e = 0$, the maximum equilibrium tem-

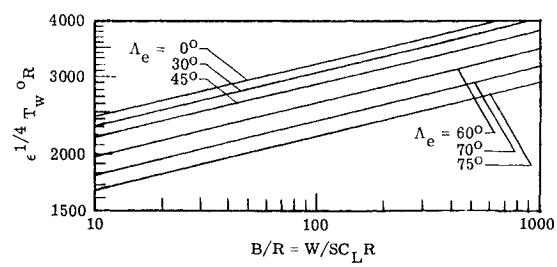

Fig. 1 Maximum stagnation-line temperatures for equilibrium-glide entry.

Received July 29, 1970; revision received September 4, 1970.

* Aerospace Engineer, Aerothermal Branch, Space Systems Research Division. Member AIAA.